iScience

CellPress

Article

Glutamate Signaling in the Fly Visual System

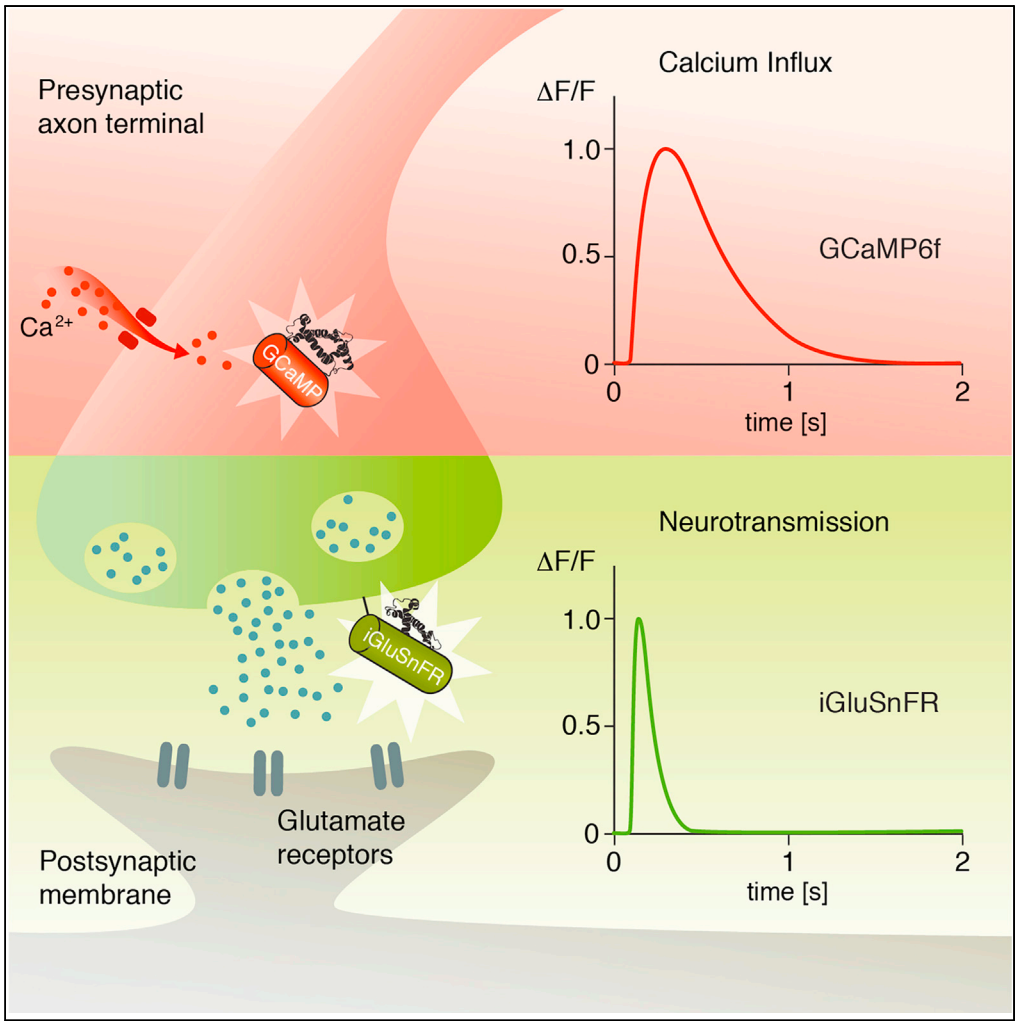

Florian G. Richter, Sandra Fendl, Jürgen Haag, Michael S. Drews, Alexander Borst

frichter@neuro.mpg.de (F.G.R.)
aborst@neuro.mpg.de (A.B.)

HIGHLIGHTS

The glutamate sensor iGluSnFR is suitable for 2-photon imaging in the fruit fly

Response properties obtained with iGluSnFR are much faster than those with GCaMP6f

Spatial aspects of receptive fields are preserved between indicators

Richter et al., iScience 7, 85–95
September 28, 2018
https://doi.org/10.1016/j.isci.2018.08.019

iScience

CellPress

Article

Glutamate Signaling in the Fly Visual System

Florian G. Richter,[1,2,*] Sandra Fendl,[1,2] Jürgen Haag,[1] Michael S. Drews,[1] and Alexander Borst[1,3,*]

SUMMARY

For a proper understanding of neural circuit function, it is important to know which signals neurons relay to their downstream partners. Calcium imaging with genetically encoded calcium sensors like GCaMP has become the default approach for mapping these responses. How well such measurements represent the true neurotransmitter output of any given cell, however, remains unclear. Here, we demonstrate the viability of the glutamate sensor iGluSnFR for 2-photon *in vivo* imaging in *Drosophila melanogaster* and prove its usefulness for estimating spatiotemporal receptive fields in the visual system. We compare the results obtained with iGluSnFR with the ones obtained with GCaMP6f and find that the spatial aspects of the receptive fields are preserved between indicators. In the temporal domain, however, measurements obtained with iGluSnFR reveal the underlying response properties to be much faster than those acquired with GCaMP6f. Our approach thus offers a more accurate description of glutamatergic neurons in the fruit fly.

INTRODUCTION

To understand how neural circuits operate and carry out certain computations, it is essential to observe the signals that are transmitted from cell to cell. Synaptic transmission via chemical synapses proceeds in four major stages: (1) Depolarization in the presynapse opens voltage-gated calcium channels. (2) The resulting calcium influx leads to the fusion of transmitter-filled vesicles and the presynaptic membrane. (3) Transmitter molecules are released into the synaptic cleft where they diffuse and bind receptors in the postsynaptic membrane. (4) The subsequent activation of these receptors leads to opening or closing of ion channels, either directly or indirectly, with the resulting ion flux ultimately changing the postsynaptic membrane conductance and potential (reviewed in [Di Maio, 2008]). This fundamental signaling cascade, from electric potential to calcium to transmitter release to postsynaptic electric potential, orchestrates computation within any neuronal circuit.

For monitoring voltage changes, electrophysiology is the default approach. Here, direct observations of both de- and hyperpolarization in pre- or postsynaptic cells are possible. Due to the position or size of many neurons, however, direct single-cell recordings are often not feasible and have to be replaced by indirect extracellular recordings or optical imaging. Only recently genetically encoded voltage indicators (GEVIs) have emerged as powerful tools for recording neuronal activity (Cao et al., 2013; Jin et al., 2012; St-Pierre et al., 2014; Tsutsui et al., 2013; Yang et al., 2016). Experiments with optical voltage indicators such as ASAP2f that are compatible with 2-photon imaging, however, remain challenging due to weak signal-to-noise ratio (Yang et al., 2016). The fluorescence level of genetically encoded calcium indicators (GECIs) is thought to correlate with transmitter release and is therefore suitable for identifying the crucial signal to the postsynaptic cell (Zucker, 1993). Although GECIs are being improved continuously and some variants were designed to have especially fast kinetics (e.g., GCaMP6f [Chen et al., 2013]), temporal resolution is still limited due to calcium buffering (Borst and Abarbanel, 2007). This usually leads to decay constants in the order of several hundreds of milliseconds that vary depending on the system under observation (Arenz et al., 2017; Chen et al., 2013). For glutamatergic neurons, a tool to potentially overcome these limitations is the recently developed fast glutamate sensor iGluSnFR (Marvin et al., 2013).

Visual motion detection is a canonical example for computation in neural microcircuits. Prevalent models posit that, in both mammalian retina and fly visual system, local direction selectivity emerges from the nonlinear interaction between precisely tuned spatiotemporal filters (Barlow and Levick, 1965; Von Hassenstein and Reichardt, 1956). Recent work in connectomics on the visual system of *Drosophila melanogaster* has revealed this computation to be implemented by a circuit that consists of only a few dozen individual cells (Takemura et al., 2017). The optic lobe is the largest neuropil in the fruit fly's brain and consists of the

[1]Max-Planck-Institute of Neurobiology, 82152 Martinsried, Germany

[2]These authors contributed equally

[3]Lead Contact

*Correspondence: frichter@neuro.mpg.de (F.G.R.), aborst@neuro.mpg.de (A.B.)

https://doi.org/10.1016/j.isci.2018.08.019

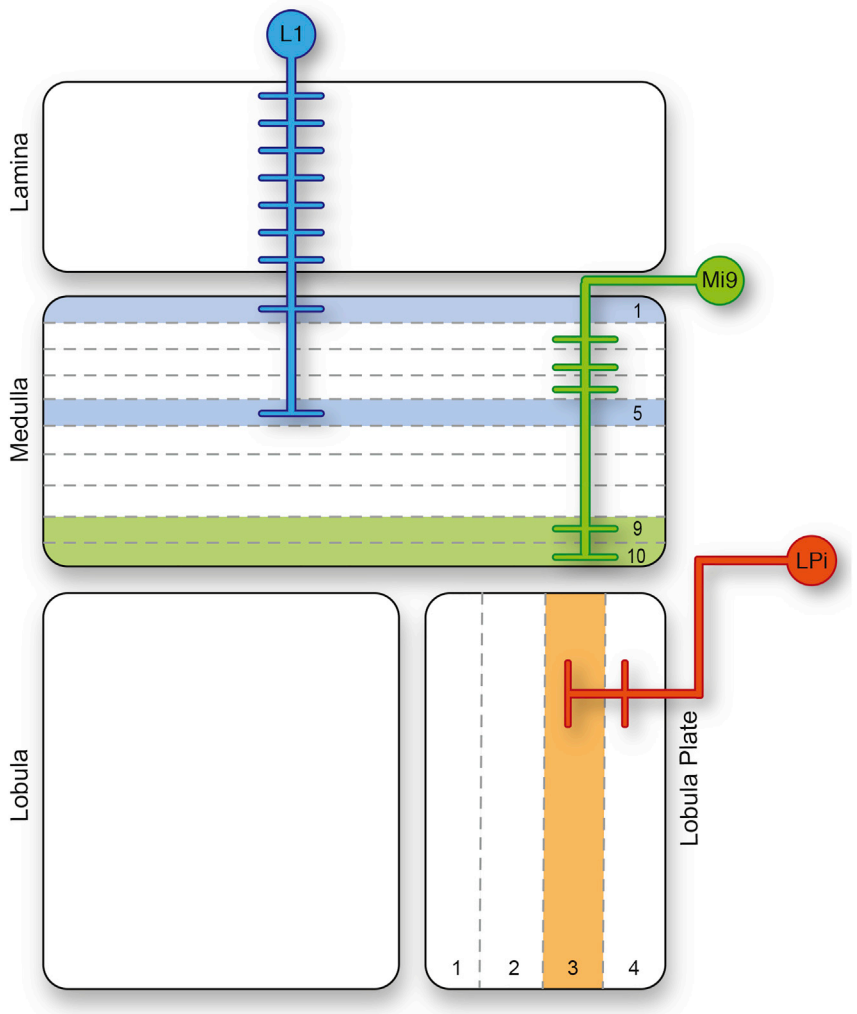

Figure 1. Schematic of the *Drosophila* Optic Lobe

Schematic of the *Drosophila* optic lobe with glutamatergic cell types in the motion vision pathway. The three cell types are not directly connected to each other but play an import role in the circuit. For the sake of simplicity, postsynaptic partners of the glutamatergic neurons are not displayed but can be reviewed in Mauss et al. (2015) and Takemura et al. (2011, 2017). Colored layers indicate area where we imaged glutamate release of the respective cell type.

four consecutive neuropils: lamina, medulla, lobula, and lobula plate (Figure 1). Lamina monopolar cells L1 and L2, among others, receive direct photoreceptor input and feed into two parallel pathways (Bausenwein et al., 1992; Bausenwein and Fischbach, 1992; Borst, 2014; Clark et al., 2011; Joesch et al., 2010; Rister et al., 2007; Shinomiya et al., 2014; Silies et al., 2013; Takemura et al., 2017; Tuthill et al., 2013). The ON pathway processes the motion of light increments, whereas the OFF pathway processes the motion of light decrements only (Eichner et al., 2011; Joesch et al., 2013, 2010). Among the medulla interneurons that connect the lamina cells to direction-selective T4 and T5 neurons (Maisak et al., 2013; Takemura et al., 2017), we find the glutamatergic cell Mi9 that has been characterized with a receptive field responsive to OFF in the center and an antagonistic ON surround (Arenz et al., 2017; Strother et al., 2017). T4 and T5 neurons each come in four subtypes, tuned to one of the four cardinal directions, and project, according to their preferred direction, to one of the four layers in the lobula plate. Here, T4 and T5 cells make excitatory cholinergic connections onto the dendrites of large tangential cells as well as onto inhibitory lobula plate interneurons (LPis). These neurons in turn inhibit large field tangential cells in the adjacent layer during null direction motion and thus increase their flow-field selectivity (Hausen et al., 1980; Hopp et al., 2014; Schnell et al., 2010; Scott et al., 2002; Wasserman et al., 2015). To provide this inhibition, LPis release glutamate onto the glutamate

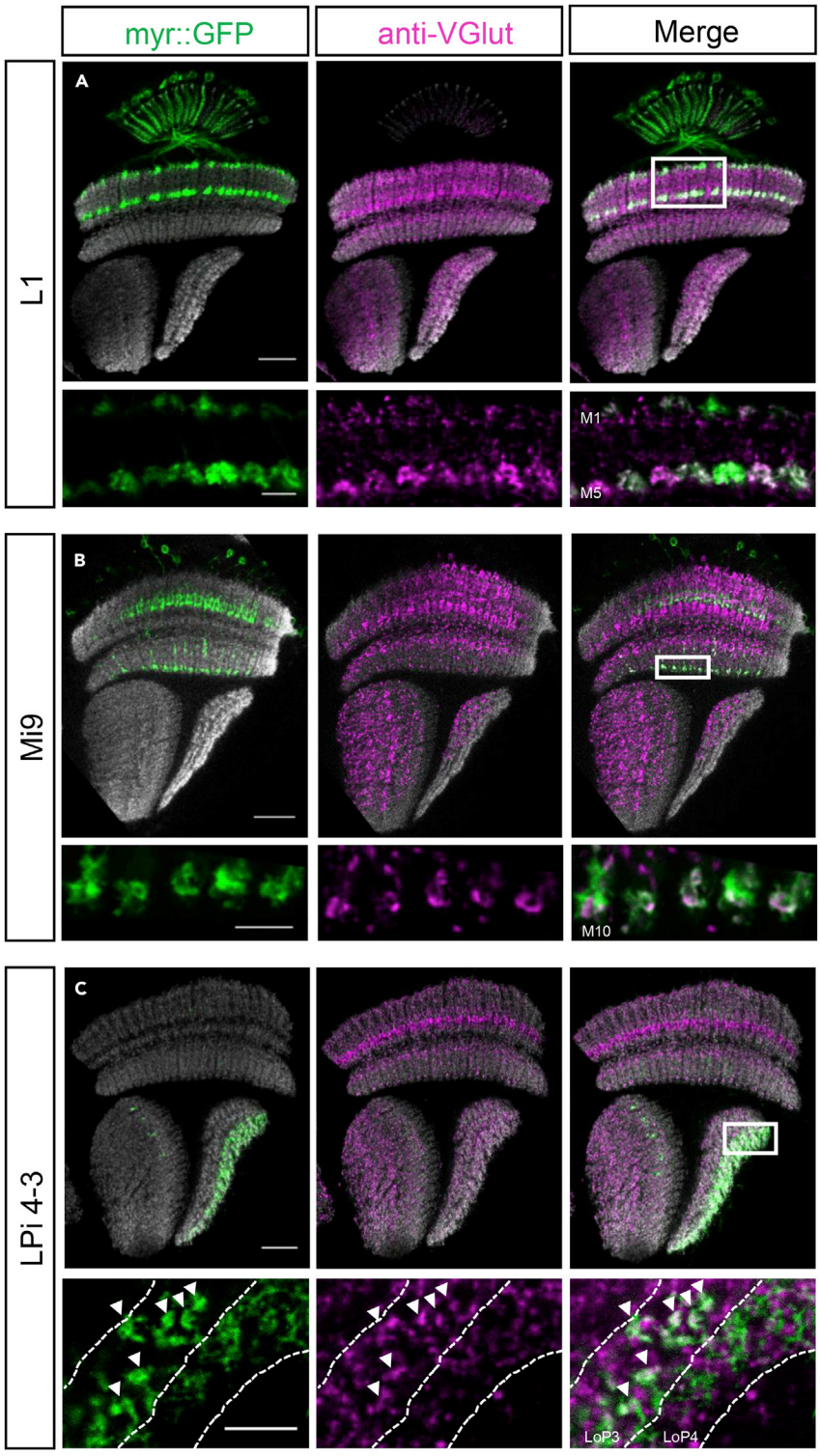

Figure 2. Vesicular Glutamate Transporter VGlut Localizes to Axon Terminals of L1, Mi9, and LPi4-3 Neurons Indicating their Glutamatergic Phenotype

(A–C) Upper rows show overviews of optic lobes with L1 (A), Mi9 (B), and LPi4-3 (C) labeled with myr::GFP (green), background staining against bruchpilot brp (gray), and anti-VGlut staining (magenta). In the lower rows higher magnifications of axon terminals of L1, Mi9, and LPi4-3 neurons are depicted (sections marked with white boxes in overview images).

Figure 2. *Continued*
(A) L1 axon terminals in medulla layers 1 and 5 show overlapping signal with anti-VGlut staining.
(B) VGlut protein co-localizes with Mi9 axons in layer 10 of the medulla.
(C) Lobula plate intrinsic neurons LPi4-3 have their dendrites in layer 4 and project their terminals to layer 3. Labeled with arrowheads are LPi boutons in layer 3 showing overlapping signal with anti-VGlut staining. Shown here are single planes of confocal stacks. Scale bar for overview of optic lobes is 20 μm. For higher magnification close-ups the scale is 5 μm. White dashed lines in the lower panel are manually drawn and indicate layers of the lobula plate.

receptor GluClα, which is an inhibitory glutamate receptor only found in invertebrates (Liu and Wilson, 2013; Mauss et al., 2015, 2014).

The exact biophysical mechanisms by which T4 and T5 become direction selective remain unclear. To understand on a cell-by-cell level how direction selectivity is achieved, precise measurements of the signals transmitted between neurons are crucial. In this study, we focus on the final stage of the synaptic signaling cascade, i.e., transmitter release. First, we confirm the neurotransmitter phenotype of all known glutamatergic cell types (L1, Mi9, LPi) in the *Drosophila* motion vision pathway. Second, using the recently developed fast glutamate sensor iGluSnFR (Marvin et al., 2013), we comprehensively characterize their spatiotemporal response profiles and compare them with the ones obtained expressing the genetically encoded calcium indicator GCaMP6f (Chen et al., 2013).

RESULTS

The Vesicular Glutamate Transporter VGlut Localizes to Axon Terminals of L1, Mi9, and LPi4-3 Neurons

VGlut or DVGLUT (CG9887) is the only vesicular glutamate transporter known in *Drosophila*. VGlut is located in the vesicle membrane of glutamatergic neurons where it fills the synaptic vesicles with glutamate. The protein localizes to presynaptic terminals of all known glutamatergic neuromuscular junctions (NMJs) as well as to synapses throughout the CNS neuropil in *Drosophila* (Daniels, 2004). Hence, VGlut is the most commonly used marker for glutamatergic neurons. Several antibodies have been raised against VGlut to identify glutamatergic neurons in the nervous system of the fruit fly (Daniels, 2004; Mahr and Aberle, 2006).

Recent studies revealed the glutamatergic phenotype of L1, Mi9, and LPi neurons—each of them a crucial element of the motion vision pathway of the fruit fly (Joesch et al., 2010; Kolodziejczyk et al., 2008; Mauss et al., 2015; Takemura et al., 2017, 2011). The somata of these cell types showed positive immunoreactivity against the VGlut antibody, which was raised against a C-terminal peptide—CQMPSYDPQGYQQQ (Daniels, 2004). Interestingly, this antibody labeled mainly cell bodies of designated neurons. Since it is known that the vesicular glutamate transporter VGlut is localized to axon terminals, we investigated the glutamatergic transmitter phenotype of L1, Mi9, and LPi4-3 in more detail. We used a different anti-VGlut antibody (Mahr and Aberle, 2006), which only labels neuronal arborizations in the optic lobe neuropil and no somata. In general, the VGlut protein is highly abundant throughout all four neuropils of the optic lobe (Figure 2).

The axon terminals of L1 neurons show clear overlap with the anti-VGlut signal in layer M1 and M5 of the medulla (Figure 2A). The vesicular glutamate transporter VGlut resides at the presynaptic sites of L1 neurons, which indicates their glutamatergic phenotype. In layer M10 of the medulla, the same is found for Mi9 neurons: VGlut staining in this layer is co-localized with GFP-labeled Mi9 axon terminals (Figure 2B). This suggests that Mi9 neurons are glutamatergic and that they are the only source of glutamate in layer M10 of the medulla. Furthermore, we found an overlapping signal of LPi4-3 terminals in layer 3 of the lobula plate and anti-VGlut staining (Figure 2C). This confirms recent findings (Mauss et al., 2015) that described LPi neurons as glutamatergic, being presynaptic only in one of the two layers where it arborizes.

In summary, we could show that the protein VGlut localizes to axon terminals of the glutamatergic neurons L1, Mi9, and LPi4-3.

Faster Sensor Kinetics Enable More Precise Characterization of Visual Interneurons

One commonly used approach to characterize a sensory neuron is to find its preferred stimulus. This can be achieved by using a white noise input and cross-correlating the resulting output with the input (Dayan and

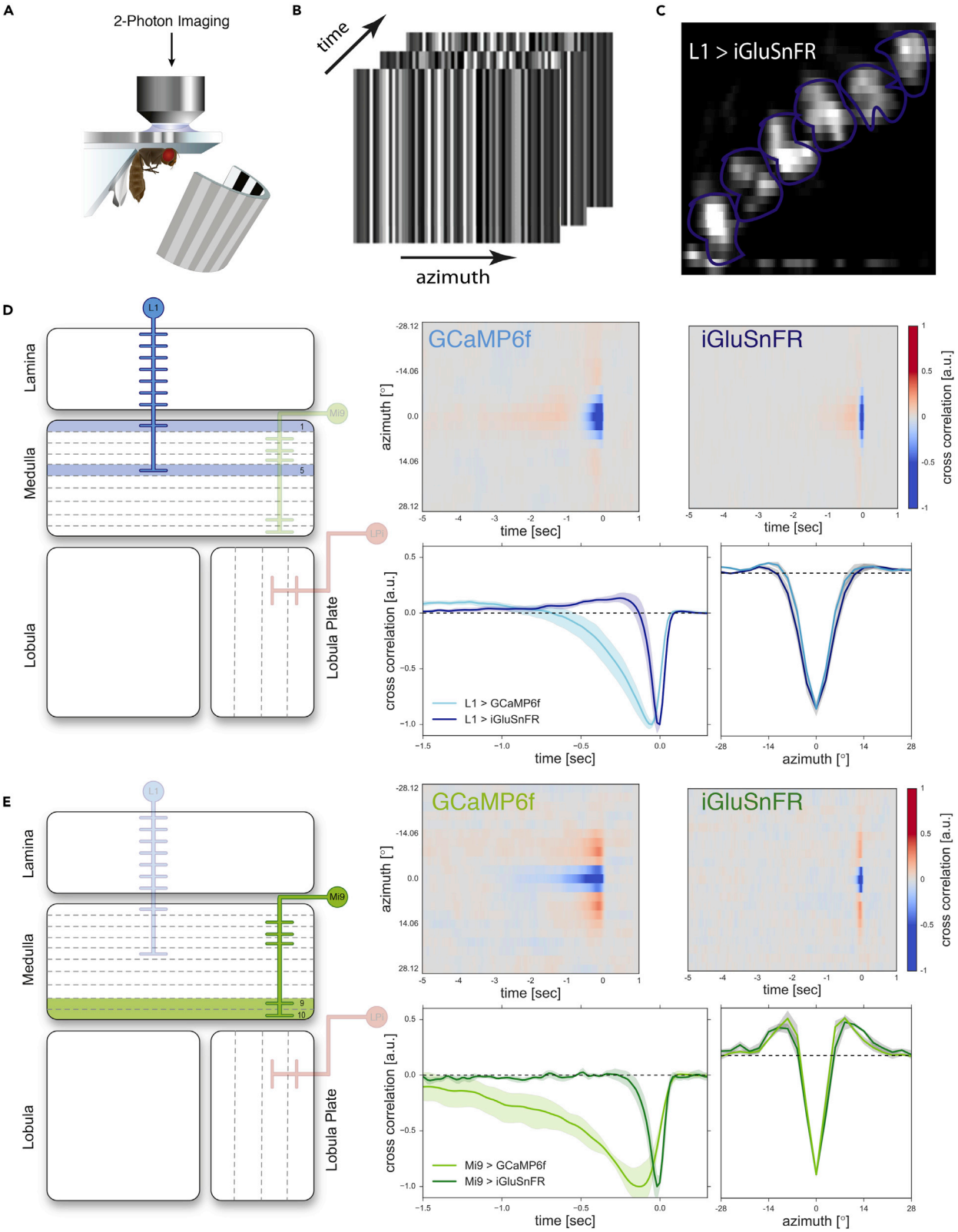
A
2-Photon Imaging
B
time
azimuth
C
L1 > iGluSnFR
D
L1
Lamina
Medulla
Lobula
Mi9
LP1
Lobula Plate
GCaMP6f
iGluSnFR
azimuth [°]
time [sec]
cross correlation [a.u.]
L1 > GCaMP6f
L1 > iGluSnFR
azimuth [°]
E
Mi9
Mi9 > GCaMP6f
Mi9 > iGluSnFR

Figure 3. Response Properties of the ON Pathway Columnar Elements L1 and Mi9

(A) Experimental setup: Fly tethered to a plastic holder under the 2-photon microscope looking onto the stimulus arena (see also Transparent Methods).

(B) Schematic of three frames of the white noise stimulus consisting of 64 horizontal bars.

(C) Example of 2-photon image of L1 expressing iGluSnFR. In purple are manually drawn region of interest ROIs.

(D) Left: Schematic of the *Drosophila* optic lobe. The cell type related to the right panel is highlighted. Right upper panel: Averaged aligned spatiotemporal receptive fields after reverse correlation of L1 expressing either the glutamate indicator iGluSnFR (5 flies and 66 cells) or GCaMP6f (5 flies and 60 cells). Cross sections along space and time axes result in receptive fields in right lower panel. Spatial receptive fields do not differ significantly for both indicators. Temporal kernels differ substantially. Impulse responses are shorter for iGluSnFR than for GCaMP6f. Shaded areas indicate a confidence interval of 95%.

(E) Same as (D) only for Mi9 (with iGluSnFR: 5 flies, 26 cells; with GCaMP6f: 5 flies, 50 cells).

Abbott, 2013; French, 1976; Ringach and Shapley, 2004), which yields the linear spatiotemporal receptive field as a result (e.g., Figures 3D and 3E, upper panel). The receptive field of a neuron is defined as the location of a stimulus in space and the time relative to its occurrence in which the neuron's response is modulated by the stimulus. The receptive field also describes the specific filtering properties of a system, in space as well as in time. Here, we use simple first-order low-pass, high-pass, or band-pass filters to quantify these filtering properties using the measured receptive fields. A low-pass filter only allows low frequencies to pass and attenuates high frequencies. Conversely, a high-pass filter attenuates low frequencies and allows high frequencies to pass. A band-pass filter is a combination of a high-pass and a low-pass filter in series, allowing signals within a certain frequency band to pass and attenuating all others (Cruse, 1996). In a linear system, the filters characterized this way are equivalent to the neurons' impulse responses. The temporal impulse response reveals critical aspects of the cellular response kinetics (Dayan and Abbott, 2013; Ringach and Shapley, 2004).

For this reason, we characterized the spatial extent of the receptive fields as well as the response dynamics of all known glutamatergic cells in the motion vision circuit of *Drosophila* L1, Mi9, and LPi4-3. Expressing either the fast version of the genetically encoded calcium indicator GCaMP6f (Chen et al., 2013) or the fast glutamate-sensing reporter iGluSnFR (Marvin et al., 2013) with cell-type-specific Gal4 driver lines, we imaged glutamate and calcium signals in single axon terminals (Figure 3C). To precisely map the receptive fields of these cells, we used a one-dimensional white noise stimulus consisting of 2.8° wide vertical bars covering the full extent of the arena (180°, Figure 3B, see also Methods). The spatiotemporal receptive fields were then determined from the neuron's calcium or glutamate response by reverse correlation. Cross sections through the peak of the spatiotemporal receptive fields along the space axis therefore yield the one-dimensional spatial receptive fields depicted in Figures 3D and 3E. Cross sections along the time axis yield the temporal filtering properties of the neuron (Chichilnisky, 2001; Dayan and Abbott, 2013; French, 1976; Ringach, 2004).

To calculate the spatial extent of the cells' receptive field, we fitted a Mexican hat function (also called difference of Gaussians) that best resembled the center-surround structure of the estimated spatial receptive fields. Both neurons show a small confined center of ~7° for Mi9 and 9–11° for L1. The full width at half maximum of the surround is about 40–50° for L1 and 20–30° for Mi9. Considering the uncertainty of the fitted model parameters, these values are similar and lie in the same order of magnitude when comparing results from imaging with both sensors. In addition, testing the raw data of both conditions against each other we find no significant difference (see Figures S2A and S2B, p value > 0.5, Welch's t test) of spatial receptive fields neither for L1 nor for Mi9. Both neurons show a small confined center of ~7° for Mi9 and 9–11° for L1. The size of the surround has the same order of magnitude for both sensors, 40–50° for L1 and 20–30° for Mi9. This is within the range of uncertainty that the fit is subject to. Testing the raw data of both conditions against each other for the two cell types, however, does not yield a significant difference (see Figures S2A and S2B, right panel).

For a reliable estimation of the time constants of the temporal responses, we transferred the impulse responses of L1 and Mi9 into frequency space and fitted either a first-order low-pass or a first-order band-pass filter to the neurons' responses (see Figures S1C and S1D). For L1, we find that the data are best represented by a band-pass filter. The filter derived from the iGluSnFR signal has a low-pass time constant of 70 ms and a high-pass time constant of about 400 ms (see Figure S1A). The time constants derived from the GCaMP6f signal are significantly larger with low-pass and high-pass time constants of 350 and about 1,180 ms, respectively. For Mi9, we find that the temporal properties are best described by a low-pass filter. The estimated time constant of the Mi9 temporal kernel (Figure 3D, lower

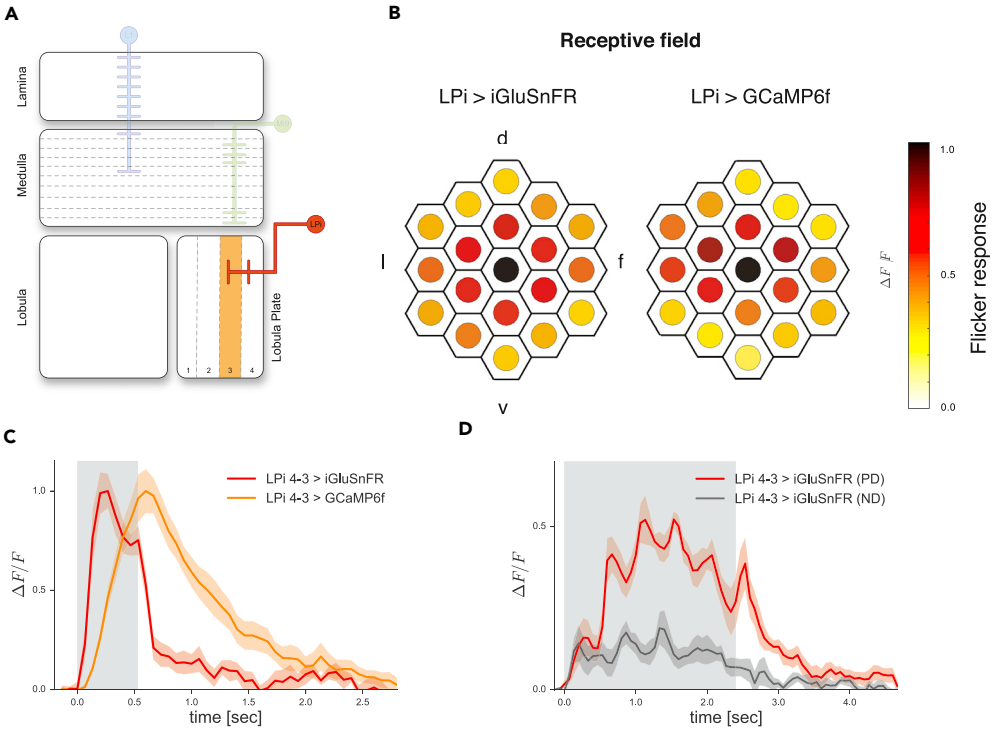

Figure 4. Response Properties of the Direction Selective Lobula Plate Interneuron LPi4-3

(A) Schematic of the *Drosophila* optic lobe with LPi4-3 highlighted.

(B) Comparison of spatial receptive field size of LPi4-3 cells recorded with iGluSnFR (left, n = 24 cells from 7 flies) or GCaMP6f (right, n = 14 cells from 5 flies). The responses of individual cells to flicker stimuli presented at 19 different columnar positions were averaged after alignment to the maximum (in black) and normalization. d, Dorsal; v, ventral; l, lateral; f, frontal.

(C) Time course of LPi4-3 response upon local flicker stimulation. The decay of the signal is faster for iGluSnFR response.

(D) LPi4-3 expressing iGluSnFR show glutamatergic direction selective responses (n = 8 cells from 5 flies). Five consecutive flicker stimuli were shown along the preferred (downward) or null (upward) direction of the neuron, acting as apparent motion. Shaded areas indicate mean ± SEM.

left) is 75 ms when measured with iGluSnFR compared with about 610 ms when measured with GCaMP6f (see Figure S1B).

For both cell types, the temporal kernel of the calcium response can be derived by low-pass filtering the faster glutamate signal. This is because the kinetics of the calcium sensor can be approximated by a low-pass filter when the intracellular calcium concentration is small compared to the KD value of the indicator (Borst and Abarbanel, 2007). For both cells, i.e., L1 and Mi9, we can fit the glutamatergic signal to the calcium signal by filtering it with a low-pass filter with a time constant of 360 ms (see Figures S2A and S2B, left panel). LPis, as motion-selective neurons, are not suitable for white noise analysis. To characterize the response properties of the LPi4-3 (Figure 4A), we first stimulated single ommatidia with local flicker stimuli that were placed precisely onto the lattice of the fly's eye via a custom-built telescopic device (see Transparent Methods and [Haag et al., 2017, 2016]). LPi4-3 cells responded to the individual pulses with different amplitudes, depending on the position of the stimulus (Figure 4C). The maximum response (Figure 4B, black center) of a recorded neuron was then set as the receptive field's center. All other responses to adjacent stimulation are normalized accordingly. Single flicker stimulations in the center of the receptive field show different time courses (Figure 4C) when using the two different indicators. The onset of the calcium response is much slower when compared with the glutamate response. In fact, whereas the glutamate signal shows a short transient peak response and then plateaus after ~500ms, the calcium signal does not resolve any similar details in the time course of the response. The calcium signal decays back to zero in approximately 2 s after stimulus offset, whereas the glutamatergic signals are back at the baseline level in less than 200 ms. This loss-of-response features can be explained by the characteristics of the

calcium indicator, which acts as a low-pass filter (Borst and Abarbanel, 2007). Low-pass filtering the glutamate response (τ = 446 ms, Figure S2C) results in a similar slope and decay as the calcium response. We also asked if the glutamatergic signal of the LPis is indeed direction selective as expected from Mauss et al. (2015). To asses this question we tested LPi4-3 cells with five light pulses of 472 ms duration positioned along the dorsoventral axis of the eye. When stimulated sequentially from dorsal to ventral (Figure 4D), the cell responded more strongly (PD, red line) than when we showed the same stimulus in the opposite direction (ND, black line, paired sample t test, p value < 0.01). We therefore conclude that the sensor is indeed also suitable for resolving glutamatergic direction-selective signals.

DISCUSSION

In this study we showed that all three investigated cell types (L1, Mi9, LPi4-3) express the vesicular transporter for glutamate, VGlut, in their axon terminals (Figure 2). To our knowledge, L1, Mi9, and LPi are the only glutamatergic cells in the *Drosophila* motion vision circuit. Two studies using either antibody stainings (Kolodziejczyk et al., 2008) a Flp-out analysis of the dvGlutCNSIII-Gal4 driver line (heat-shock inducible flipase excises stop-cassette upstream of mCD8-GFP to label only a few cells) (Raghu and Borst, 2011) found L2 cells to be glutamatergic. However, a recent RNA sequencing study that characterized gene expression patterns of more than 60 different cell types of the optic lobe could not confirm the expression of VGlut in L2 (Davis et al., 2018). Although they could identify other cell types like Dm cells, Lai, PB_1, Tm29, and TmY5a as glutamatergic due to their expression of VGlut, none of the other cells in the motion vision circuit (besides L1, Mi9, and LPi) seem to express VGlut. The role of Dm, Lai, PB, Tm29, and TmY5a cells in general and their potential contribution to motion vision in the fly brain are not known to date.

We also demonstrated that the spatial receptive fields measured with the glutamate sensor iGluSnFR are almost identical to the ones measured with the calcium sensor GCaMP6f (Figures 3 and 4). Both neurons possess a local OFF center receptive field with a differently strong antagonistic ON surround. Surround inhibition is a phenomenon frequently found in the early processing stages in visual systems: Bipolar and ganglion cells of the mammalian retina possess receptive fields with an antagonistic center-surround structure (reviewed in Shapley and Lennie, 1985), and first-order interneurons of the insect compound eye share this feature as well (Srinivasan et al., 1982). Functionally, a neuron with a center-surround antagonism acts as a spatial band-pass filter, enhancing the neuron's responses to edges over full field illuminations. Such band-pass filtering reduces redundancy in natural images (Srinivasan et al., 1982). We find such spatial band-pass characteristics for both cell types, L1 and Mi9. Based on their spatial receptive fields, we predict, for instance, no response of Mi9 to wide field dark flashes since the integral of the spatial receptive field is close to zero.

In the time domain, however, the glutamate signal turned out to be much faster than the calcium signal derived from the same cells. Due to their small size, many visual interneurons in the fly brain are inaccessible to electrophysiological recordings, so only a few direct recordings have been reported (Behnia et al., 2014; Gruntman et al., 2018; Juusola et al., 2016). Since data from voltage recordings from L1, Mi9, and LPi are not available so far, a direct comparison with the time constant estimated here is not possible. Simulation studies predicted time constants between 50 and 100 ms for the delayed input to the fly motion-detecting neurons (Eichner et al., 2011; Leonhardt et al., 2016). Since Mi9 is thought to provide this signal to T4 cells, the elementary motion-sensing neurons in the ON pathway, the low-pass time constant of 75 ms estimated here matches this prediction well. In addition, a previous study determined the low-pass time constant for Mi9 to be around 550 ms from calcium imaging experiments. A deconvolution of the filter with an estimated GCaMP kernel led to a resulting time constant of 63 ms (Arenz et al., 2017). This result again is in line with the time constants of the Mi9-iGluSnFR of 75 ms reported here.

In the mammalian CNS, glutamate is the most abundant and major excitatory transmitter (Meldrum, 2000; Traynelis et al., 2010). Glutamate binds to two types of receptors: metabotropic (mGluRs) and ionotropic glutamate receptors (iGluRs). iGluRs can be divided into N-methyl-D-aspartate (NMDA) and non-NMDA receptors (α-amino-3-hydroxy-5-methyl-4-isoxazolepropionic acid [AMPA] and kainate receptors) according to their response to agonist molecules NMDA and AMPA (Mosbacher et al., 1994). Analysis of the *Drosophila* genome annotated 14 iGluRs genes, which show sequence similarities with vertebrate AMPA, kainite, and NMDA receptors (Littleton and Ganetzky, 2000). However, the kainite receptor DKaiR1D and the AMPA receptor DGluR1A have different agonist/antagonist selectivity from the vertebrate's pharmacology-based classification (Li et al., 2016). Furthermore, invertebrates like *Drosophila melanogaster* possess a third type of iGluR, the so-called glutamate-gated chloride channel GluClα, which

is inhibitory (Cully et al., 1996; Liu and Wilson, 2013). Glutamate can also act on metabotropic glutamate receptors, which signal via slower G-protein-coupled pathways. In mammals, eight mGluRs have been described (Conn and Pin, 1997). In contrast, the *Drosophila* genome encodes only one functional mGluR (DmGluRA), which is expressed at the glutamatergic NMJ localized in the presynaptic boutons (Bogdanik et al., 2004). Regarding the broad range of glutamate receptors in *Drosophila*, glutamate can act as a fast, slow, excitatory, or inhibitory transmitter (Li et al., 2016; Liu and Wilson, 2013; Mauss et al., 2015).

This gives rise to interesting speculations about the respective role of glutamate for each of the cell types investigated. In the case of the LPis, glutamate binds to the inhibitory glutamate receptor GluClα on the dendrites of large-field tangential cells, inhibiting them during null direction motion and, thus, enhancing their flow-field selectivity (Mauss et al., 2015). In the case of L1, the glutamatergic output signal seems to be key for the sign inversion of L1's OFF response in the ON pathway. This is because all *Drosophila* photoreceptors (R1-R8) depolarize upon illumination and release histamine onto lamina neurons, which results in the opening of chloride channels (Hardie, 1989; Hardie and Raghu, 2001). Therefore, lamina monopolar cells transiently hyperpolarize upon illumination onset and respond with a rebound excitation at illumination offset (Laughlin et al., 1987). L1 and L2 neurons respond in an identical way (Joesch et al., 2010). L1 possess an OFF receptive field center (Figure 3D) and therefore depolarizes to OFF stimuli, in contrast to its described downstream synaptic partners, which depolarize to ON stimuli (Arenz et al., 2017; Behnia et al., 2014; Strother et al., 2017; Yang et al., 2016). Hence, an inversion of the sign must occur at the synapse of L1 and its downstream partners. Since L1 is glutamatergic and GluClα is the only inhibitory receptor described in *Drosophila*, the glutamatergic signal is likely to be responsible for this sign inversion. Whether the downstream partners of L1 indeed express GluClα, however, is beyond the scope of this study and awaits further investigation. The hypothesis outlined above suggests that the mechanism by which a common photoreceptor input signal is split into an ON and an OFF pathway in invertebrates is different from the one in the mammalian retina where glutamatergic photoreceptors hyperpolarize in response to light. This signal is directly transmitted, i.e., without sign inversion, by ionotropic glutamate receptors expressed on the dendrites of OFF bipolar cells (Euler et al., 2014) and sign inverted by metabotropic glutamate receptors expressed on the dendrites of ON bipolar cells (Masu et al., 1995). In case of Mi9, the functional interpretation of an inhibitory glutamatergic signal is less intuitive. Mi9 directly contacts the dendrites of T4 cells, the first direction-selective neurons in the ON pathway (Takemura et al., 2017). Given the OFF response of Mi9 cells (Figure 3D), T4 cells are expected to be inhibited in darkness via the Mi9-T4 synapse. A moving ON edge would inhibit Mi9 followed by a closure of chloride channels and, thus, an increased input resistance in postsynaptic T4 cells, resulting in an amplification of a subsequently delivered excitatory input signal. Computer simulations have shown that such a two-fold signal inversion can indeed form the biophysical basis of preferred direction enhancement underlying direction selectivity in T4 cells (Borst, 2018).

Taken together our results could demonstrate the functionality of the fast glutamate reporter iGluSnFR in glutamatergic neurons of the fruit fly *Drosophila melanogaster*. It allowed for a more faithful description of important elements of the motion vision pathway, in particular with respect to their temporal response properties.

Limitations of the Study

Since iGluSnFR is anchored to the outer side of the plasma membrane, it senses extracellular glutamate that is present in the synaptic cleft. In addition, the iGluSnFR signal is affected by spillover and diffusion to iGluSnFR molecules outside the cleft. Thus, the iGluSnFR signal should present an upper limit to the "real" time course, i.e., the one of glutamate in the synaptic cleft as seen by the postsynaptic receptors. For the same reason, one might record an iGluSnFR signal even if the indicator is expressed on a neuron that is not glutamatergic or does not receive glutamatergic input, but ramifies within the same volume where glutamate is being released from other cells.

METHODS

All methods can be found in the accompanying Transparent Methods supplemental file.

SUPPLEMENTAL INFORMATION

Supplemental Information includes Transparent Methods and two figures and can be found with this article online at https://doi.org/10.1016/j.isci.2018.08.019.

ACKNOWLEDGMENTS

We thank Aljoscha Leonhardt for careful proofreading of the manuscript. We would also like to acknowledge Hermann Aberle for sharing the VGlut antibody with us and Julia Kuhl for designing the graphical abstract. We thank Wolfgang Essbauer and Michael Sauter for fly husbandry. This work was supported by the Deutsche Forschungsgemeinschaft (SFB 870) and the Max Planck Society. F.G.R., M.S.D., S.F., and A.B. are members of the Graduate School of Systemic Neurosciences (GSN) Munich.

AUTHOR CONTRIBUTIONS

F.G.R., S.F., and A.B. conceived the study and designed the experiments. F.G.R. conducted and analyzed the imaging experiments for Mi9 and L1. S.F. performed and analyzed all stainings. J.H. performed and analyzed the LPi experiments. M.S.D. performed data analysis and model fitting of the receptive fields. F.G.R. wrote the manuscript with the help of all authors.

DECLARATION OF INTERESTS

The authors declare no competing interests.

Received: July 5, 2018
Revised: August 13, 2018
Accepted: August 23, 2018
Published: September 28, 2018

REFERENCES

Arenz, A., Drews, M.S., Richter, F.G., Ammer, G., and Borst, A. (2017). The temporal tuning of the *Drosophila* motion detectors is determined by the dynamics of their input elements. Curr. Biol. *27*, 929–944.

Barlow, H.B., and Levick, W.R. (1965). The mechanism of directionally selective units in rabbit's retina. J. Physiol. *178*, 477–504.

Bausenwein, B., Dittrich, A.P.M., and Fischbach, K.F. (1992). The optic lobe of *Drosophila melanogaster* - II. Sorting of retinotopic pathways in the medulla. Cell Tissue Res. *267*, 17–28.

Bausenwein, B., and Fischbach, K.F. (1992). Activity labeling patterns in the medulla of *Drosophila melanogaster* caused by motion stimuli. Cell Tissue Res. *270*, 25–35.

Behnia, R., Clark, D.A., Carter, A.G., Clandinin, T.R., and Desplan, C. (2014). Processing properties of ON and OFF pathways for *Drosophila* motion detection. Nature *512*, 427–430.

Bogdanik, L., Mohrmann, R., Ramaekers, A., Bockaert, J., Grau, Y., Broadie, K., and Parmentier, M.L. (2004). The *Drosophila* metabotropic glutamate receptor DmGluRA regulates activity-dependent synaptic facilitation and fine synaptic morphology. J. Neurosci. *24*, 9105–9116.

Borst, A. (2018). A biophysical mechanism for preferred direction enhancement in fly motion vision. PLoS Comput. Biol. *14* (6), e1006240.

Borst, A. (2014). In search of the holy grail of fly motion vision. Eur. J. Neurosci. *40*, 3285–3293.

Borst, A., and Abarbanel, H.D. (2007). Relating a calcium indicator signal to the unperturbed calcium concentration time-course. Theor. Biol. Med. Model. *4*, 7.

Cao, G., Platisa, J., Pieribone, V.A., Raccuglia, D., Kunst, M., and Nitabach, M.N. (2013). Genetically targeted optical electrophysiology in intact neural circuits. Cell *154*, 904–913.

Chen, T.-W., Wardill, T.J., Sun, Y., Pulver, S.R., Renninger, S.L., Baohan, A., Schreiter, E.R., Kerr, R.A., Orger, M.B., Jayaraman, V., et al. (2013). Ultrasensitive fluorescent proteins for imaging neuronal activity. Nature *499*, 295–300.

Chichilnisky, E.J. (2001). A simple white noise analysis of neuronal light responses. Network *12*, 199–213.

Clark, D.A., Bursztyn, L., Horowitz, M.A., Schnitzer, M.J., and Clandinin, T.R. (2011). Defining the computational structure of the motion detector in *Drosophila*. Neuron *70*, 1165–1177.

Conn, P.J., and Pin, J.-P. (1997). Pharmacology and function of metabotropic glutamate receptors. Annu. Rev. Pharmacol. Toxicol. *37*, 205–237.

Cruse, H. (1996). Neural Networks as Cybernetics Systems.

Cully, D.F., Paress, P.S., Liu, K.K., Schaeffer, J.M., and Arena, J.P. (1996). Identification of a *Drosophila melanogaster* glutamate-gated chloride channel sensitive to the antiparasitic agent avermectin. J. Biol. Chem. *271*, 20187–20191.

Daniels, R.W. (2004). Increased expression of the *Drosophila* vesicular glutamate transporter leads to excess glutamate release and a compensatory decrease in quantal content. J. Neurosci. *24*, 10466–10474.

Davis, F.P., Nern, A., Picard, S., Reiser, M.B., Rubin, G.M., Eddy, S.R., and Henry, G.L. (2018). A genetic, genomic, and computational resource for exploring neural circuit function. bioRxiv. https://doi.org/10.1101/385476.

Dayan, P., and Abbott, L.F. (2013). Theoretical neuroscience: computational and mathematical modeling of neural systems. J. Chem. Inf. Model. *53*, 1689–1699.

Di Maio, V. (2008). Regulation of information passing by synaptic transmission: a short review. Brain Res. *1225*, 26–38.

Eichner, H., Joesch, M., Schnell, B., Reiff, D.F., and Borst, A. (2011). Internal structure of the fly elementary motion detector. Neuron *70*, 1155–1164.

Euler, T., Haverkamp, S., Schubert, T., and Baden, T. (2014). Retinal bipolar cells: elementary building blocks of vision. Nat. Rev. Neurosci. *15*, 507–519.

French, A.S. (1976). Practical nonlinear system analysis by Wiener kernel estimation in the frequency domain. Biol. Cybern. *24*, 111–119.

Gruntman, E., Romani, S., and Reiser, M.B. (2018). Simple integration of fast excitation and offset, delayed inhibition computes directional selectivity in *Drosophila*. Nat. Neurosci. *21*, 250–257.

Haag, J., Arenz, A., Serbe, E., Gabbiani, F., and Borst, A. (2016). Complementary mechanisms create direction selectivity in the fly. Elife *5*, https://doi.org/10.7554/eLife.17421e.

Haag, J., Mishra, A., and Borst, A. (2017). A common directional tuning mechanism of *Drosophila* motion-sensing neurons in the ON and in the OFF pathway. Elife *6*, 1–15.

Hardie, R.C. (1989). A histamine-activated chloride channel involved in neurotransmission at a photoreceptor synapse. Nature *339*, 704–706.

Hardie, R.C., and Raghu, P. (2001). Visual transduction in *Drosophila*. Nature *413*, 186–193.

Hausen, K., Wolburg-Buchholz, K., and Ribi, W.A. (1980). The synaptic organization of visual interneurons in the lobula complex of flies - a light and electron microscopical study using silver-intensified cobalt-impregnations. Cell Tissue Res. *208*, 371–387.

Hopp, E., Borst, A., and Haag, J. (2014). Subcellular mapping of dendritic activity in optic flow processing neurons. J. Comp. Physiol. A Neuroethol. Sens. Neural Behav. Physiol. *200*, 359–370.

Jin, L., Han, Z., Platisa, J., Wooltorton, J.R.A., Cohen, L.B., and Pieribone, V.A. (2012). Single action potentials and subthreshold electrical events imaged in neurons with a fluorescent protein voltage probe. Neuron *75*, 779–785.

Joesch, M., Schnell, B., Raghu, S.V., Reiff, D.F., and Borst, A. (2010). ON and OFF pathways in *Drosophila* motion vision. Nature *468*, 300–304.

Joesch, M., Weber, F., Eichner, H., and Borst, A. (2013). Functional specialization of parallel motion detection circuits in the fly. J. Neurosci. *33*, 902–905.

Juusola, M., Dau, A., Zheng, L., and Rien, D. (2016). Electrophysiological method for recording intracellular voltage responses of *Drosophila* photoreceptors and interneurons to light stimuli in vivo. J. Vis. Exp. *112*, 1–16.

Kolodziejczyk, A., Sun, X., Meinertzhagen, I.A., and Nässel, D.R. (2008). Glutamate, GABA and acetylcholine signaling components in the lamina of the *Drosophila* visual system. PLoS One *3*, e2110.

Laughlin, S.B., Howard, J., and Blakeslee, B. (1987). Synaptic limitations to contrast coding in the retina of the blowfly *Calliphora*. Proc. R. Soc. Lond. B Biol. Sci. *231*, 437–467.

Leonhardt, A., Ammer, G., Meier, M., Serbe, E., Bahl, A., and Borst, A. (2016). Asymmetry of *Drosophila* ON and OFF motion detectors enhances real-world velocity estimation. Nat. Neurosci. *19*, 706–715.

Li, Y., Dharkar, P., Han, T.H., Serpe, M., Lee, C.H., and Mayer, M.L. (2016). Novel functional properties of *Drosophila* CNS glutamate receptors. Neuron *92*, 1036–1048.

Littleton, J.T., and Ganetzky, B. (2000). Ion channels and synaptic organization: analysis of the *Drosophila* genome. Neuron *26*, 35–43.

Liu, W.W., and Wilson, R.I. (2013). Glutamate is an inhibitory neurotransmitter in the *Drosophila* olfactory system. Proc. Natl. Acad. Sci. USA *110*, 10294–10299.

Mahr, A., and Aberle, H. (2006). The expression pattern of the *Drosophila* vesicular glutamate transporter: a marker protein for motoneurons and glutamatergic centers in the brain. Gene Expr. Patterns *6*, 299–309.

Maisak, M.S., Haag, J., Ammer, G., Serbe, E., Meier, M., Leonhardt, A., Schilling, T., Bahl, A., Rubin, G.M., Nern, A., et al. (2013). A directional tuning map of *Drosophila* elementary motion detectors. Nature *500*, 212–216.

Marvin, J.S., Borghuis, B.G., Tian, L., Cichon, J., Harnett, M.T., Akerboom, J., Gordus, A., Renninger, S.L., Chen, T.W., Bargmann, C.I., et al. (2013). An optimized fluorescent probe for visualizing glutamate neurotransmission. Nat. Methods *10*, 162–170.

Masu, M., Iwakabe, H., Tagawa, Y., Miyoshi, T., Yamashita, M., Fukuda, Y., Sasaki, H., Hiroi, K., Nakamura, Y., Shigemoto, R., et al. (1995). Specific deficit of the ON response in visual transmission by targeted disruption of the mGluR6 gene. Cell *80*, 757–765.

Mauss, A.S., Meier, M., Serbe, E., and Borst, A. (2014). Optogenetic and pharmacologic dissection of feedforward inhibition in *Drosophila* motion vision. J. Neurosci. *34*, 2254–2263.

Mauss, A.S., Pankova, K., Arenz, A., Nern, A., Rubin, G.M., and Borst, A. (2015). Neural circuit to integrate opposing motions in the visual field. Cell *162*, 351–362.

Meldrum, B.S. (2000). Glutamate as a neurotransmitter in the brain: review of physiology and pathology. J. Nutr. *130*, 1007S–1015S.

Mosbacher, J., Schoepfer, R., Monyer, H., Burnashev, N., Seeburg, P., and Ruppersberg, J. (1994). A molecular determinant for submillisecond desensitization in glutamate receptors. Science *266*, 1059–1062.

Raghu, S.V., and Borst, A. (2011). Candidate glutamatergic neurons in the visual system of *Drosophila*. PLoS One. https://doi.org/10.1371/journal.pone.0019472.

Ringach, D., and Shapley, R. (2004). Reverse correlation in neurophysiology. Cognit. Sci. *28*, 147–166.

Ringach, D.L. (2004). Mapping receptive fields in primary visual cortex. J. Physiol. *558*, 717–728.

Rister, J., Pauls, D., Schnell, B., Ting, C.Y., Lee, C.H., Sinakevitch, I., Morante, J., Strausfeld, N.J., Ito, K., and Heisenberg, M. (2007). Dissection of the peripheral motion channel in the visual system of *Drosophila melanogaster*. Neuron *56*, 155–170.

Schnell, B., Joesch, M., Forstner, F., Raghu, S.V., Otsuna, H., Ito, K., Borst, A., and Reiff, D.F. (2010). Processing of horizontal optic flow in three visual interneurons of the *Drosophila* brain. J. Neurophysiol. *103*, 1646–1657.

Scott, E.K., Raabe, T., and Luo, L. (2002). Structure of the vertical and horizontal system neurons of the lobula plate in *Drosophila*. J. Comp. Neurol. *454*, 470–481.

Shapley, R., and Lennie, P. (1985). Spatial frequency analysis in the visual system. Annu. Rev. Neurosci. *8*, 547–583.

Shinomiya, K., Karuppudurai, T., Lin, T.Y., Lu, Z., Lee, C.H., and Meinertzhagen, I.A. (2014). Candidate neural substrates for OFF edge motion detection in *Drosophila*. Curr. Biol. *24*, 1062–1070.

Silies, M., Gohl, D.M., Fisher, Y.E., Freifeld, L., Clark, D.A., and Clandinin, T.R. (2013). Modular use of peripheral input channels tunes motion-detecting circuitry. Neuron *79*, 111–127.

Srinivasan, M.V., Laughlin, S.B., and Dubs, A. (1982). Predictive coding: a fresh view of inhibition in the retina. Proc. R. Soc. Lond. B Biol. Sci. *216*, 1471–2954.

St-Pierre, F., Marshall, J.D., Yang, Y., Gong, Y., Schnitzer, M.J., and Lin, M.Z. (2014). High-fidelity optical reporting of neuronal electrical activity with an ultrafast fluorescent voltage sensor. Nat. Neurosci. *17*, 884–889.

Strother, J.A., Wu, S.T., Wong, A.M., Nern, A., Rogers, E.M., Le, J.Q., Rubin, G.M., and Reiser, M.B. (2017). The emergence of directional selectivity in the visual motion pathway of *Drosophila*. Neuron *94*, 168–182.

Takemura, S.Y., Nern, A., Chklovskii, D.B., Scheffer, L.K., Rubin, G.M., and Meinertzhagen, I.A. (2017). The comprehensive connectome of a neural substrate for 'ON' motion detection in *Drosophila*. Elife *6*, 1–16.

Takemura, S.Y., Karuppudurai, T., Ting, C.Y., Lu, Z., Lee, C.H., and Meinertzhagen, I.A. (2011). Cholinergic circuits integrate neighboring visual signals in a *Drosophila* motion detection pathway. Curr. Biol. *21*, 2077–2084.

Traynelis, S.F., Wollmuth, L.P., McBain, C.J., Menniti, F.S., Vance, K.M., Ogden, K.K., Hansen, K.B., Yuan, H., Myers, S.J., and Dingledine, R. (2010). Glutamate receptor ion channels: structure, regulation, and function. Pharmacol. Rev. *62*, 405–496.

Tsutsui, H., Jinno, Y., Tomita, A., Niino, Y., Yamada, Y., Mikoshiba, K., Miyawaki, A., and Okamura, Y. (2013). Improved detection of electrical activity with a voltage probe based on a voltage-sensing phosphatase. J. Physiol. *591*, 4427–4437.

Tuthill, J.C., Nern, A., Holtz, S.L., Rubin, G.M., and Reiser, M.B. (2013). Contributions of the 12 neuron classes in the fly lamina to motion vision. Neuron *79*, 128–140.

Von Hassenstein, B., and Reichardt, W. (1956). Systemtheoretische Analyse der Zeit-, Reihenfolgen-und Vorzeichenauswertung bei der Bewegungsperzeption des Rüsselkäfers Chlorophanus. Sect. B J. Chem. Sci. *11*, 513–524.

Wasserman, S.M., Aptekar, J.W., Lu, P., Nguyen, J., Wang, A.L., Keles, M.F., Grygoruk, A., Krantz, D.E., Larsen, C., and Frye, M.A. (2015). Olfactory neuromodulation of motion vision circuitry in *Drosophila*. Curr. Biol. *25*, 467–472.

Yang, H.H., St-Pierre, F., Sun, X., Ding, X., Lin, M.Z., and Clandinin, T.R. (2016). Subcellular imaging of voltage and calcium signals reveals neural processing in vivo. Cell *166*, 245–257.

Zucker, R.S. (1993). Calcium and transmitter release. J. Physiol. Paris *87*, 25–36.

ISCI, Volume 7

Supplemental Information

Glutamate Signaling in the Fly Visual System

Florian G. Richter, Sandra Fendl, Jürgen Haag, Michael S. Drews, and Alexander Borst

Supplemental Information

Supplemental Figures

A

L1	GCaMP6f	iGluSnFR
τ_{LP}	350 ms	70 ms
τ_{HP}	1178 ms	407 ms
$FWHM_{cen}$	8.74	10.56
$FWHM_{sur}$	56.55	42.55
A_{rel}	19.33	20.51

B

Mi9	GCaMP6f	iGluSnFR
τ_{LP}	607 ms	75 ms
$FWHM_{cen}$	6.69	7.18
$FWHM_{sur}$	19.37	25.86
A_{rel}	2.81	3.56

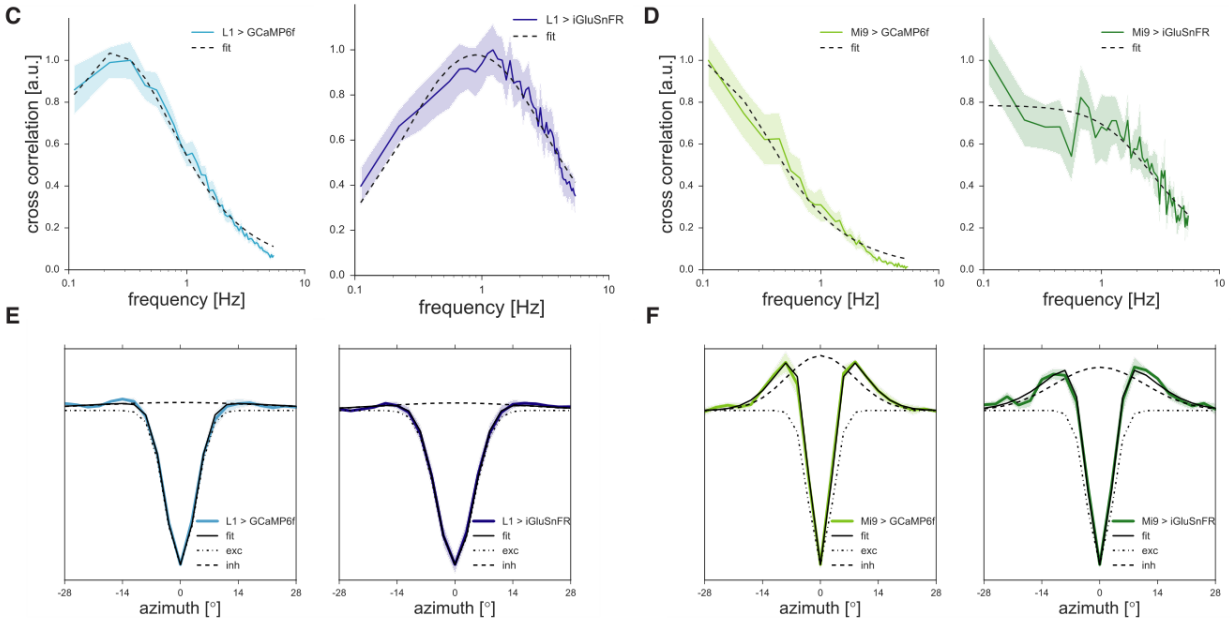

Figure S1. Model fits to L1 and Mi9 data, related to Fig 3
(A) Parameters to quantitatively describe the receptive field characteristics of L1 recorded either with GCaMP6f (left column) or iGluSnFR (right column). First two parameters describe temporal components of the receptive field, last three parameters describe those of the spatial component.
(B) Same as (A) only for Mi9. Description of highpass characteristics is missing, since Mi9 is best described by a pure low-pass.
(C) Impulse responses from Figure 3 D-E plotted in frequency space. Black dashed lines mark the fit of a 1st order band-pass filter (for time constants see table (A).
(D) Same as (C) only for Mi9. Black dashed lines mark the fit of a 1st order low-pass filter.
(E)+(F) Spatial receptive fields from Figure 3 D-E. Data are fitted with a Mexican hat function that captures both, the excitatory center as well as the inhibitory surround of these receptive fields. cen = center, sur = surround, LP = low-pass, HP = high-pass, A = amplitude, τ = time constant, FHWM = full width at half maximum.

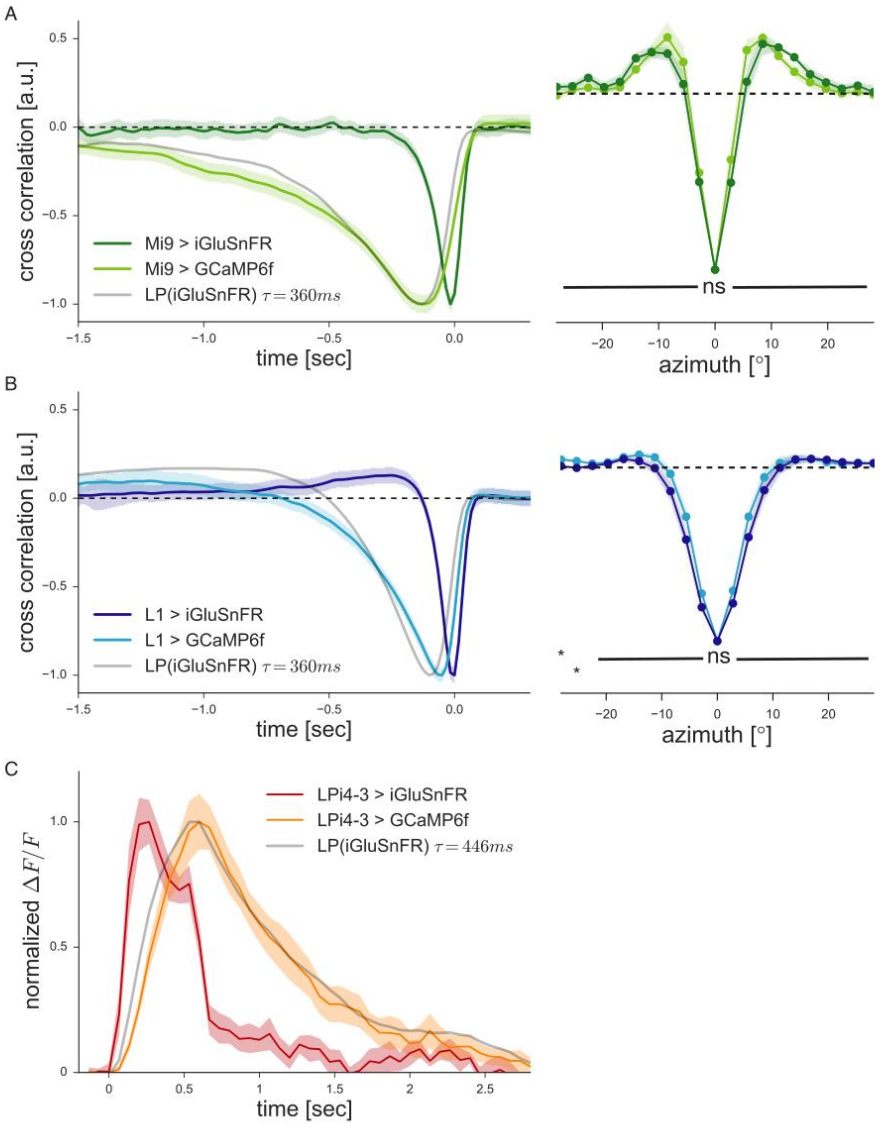

Figure S2. GCaMP data resembles low-pass filtered iGluSnFR data, related to Fig 3 and 4
(A) Low-pass filtering of the Mi9 impulse response measured with iGluSnFR with a time constant of 360 ms (grey) shows the best fit with the impulse response measured with GCaMP6f (left panel). Spatial receptive fields (right panel) are not significantly different from each other, when measured with the two different sensors.
(B) Same as (A) for L1
(C) Low-pass filtering of the LPi4-3 > iGluSnFR response to local flicker with a time constant of 446 ms (grey) shows the best fit to response measured with GCaMP6f (orange).

Transparent Methods

Flies/preparation

Flies were raised and kept on standard cornmeal-agar medium on a 12 hour light/12 hour dark cycle at 25°C and 60% humidity. For imaging experiments, the genetically-encoded calcium indicators GCaMP6f or the genetically encoded glutamate sensor iGluSnFR (Chen et al., 2013; Marvin et al., 2013) were expressed using the Gal4-UAS system in cell-type specific Gal4 fly lines, resulting in the following genotypes:

Genotypes:

L1>GC6f:	w+; R48A08-AD/UAS-GCaMP6f; R66A01-DBD/UAS-GCaMP6f
L1>iGluSnFR:	w+; R48A08-AD/+; R66A01-DBD/UAS-iGluSnFR (BL59611, AV184)
Mi9>GC6f:	w+; R48A07-AD/UAS-GCaMP6f; VT046779-DBD/UAS-GCaMP6f
Mi9>iGluSnFR:	w+; R48A07-AD/+; VT046779-DBD/UAS-iGluSnFR (BL59611, AV184)
LPi>GC6f:	w+; +/UAS-GCaMP6f; R38G02-Gal4/UAS-GCaMP6f
LPi>iGluSnFR:	w+; +; R38G02-Gal4/UAS-iGluSnFR (BL59611, AV184)

For immunohistochemical stainings in Figure 2:

L1>myr::GFP:	w-; R48A08-AD/UAS-myr::GFP; R66A01-DBD/+
Mi9>myr::GFP:	w-; R48A07-AD/ UAS-myr::GFP; VT046779-DBD/+
LPi4-3>myr::GFP:	w-; UAS-myr::GFP/+; R38G02-Gal4/+

The transgenic fly lines driving split-Gal4 expression in the lamina neuron L1 were generated and described in (Tuthill et al., 2013). Mi9 in (Strother et al., 2017) and the one of LPi's in (Mauss et al., 2015). For calcium and glutamate imaging experiments, flies were prepared as previously described (Maisak et al., 2013; Strother et al., 2017). Briefly, flies were anaesthetized on ice, fixed with their backs, legs and wings to a Plexiglas holder with the back of the head exposed to a recording chamber filled with fly external solution. The cuticle at the back of the head on one side was cut away with a fine hypodermic needle and removed together with muscles and air sacks covering the underlying optic lobe.

Data acquisition and analysis:

Data analysis was performed offline using custom-written routines in Matlab and Python 2.7 (with the SciPy and OpenCV-Python Libraries).

2-photon imaging:

Imaging was performed on custom-built 2-photon microscopes as previously described (Maisak et al., 2013) and controlled with the ScanImage software in Matlab (Pologruto et al., 2003). Acquisition rates were between 15 (for LPi experiments) and 23.67 Hz (for L1 and Mi9 experiments), image resolution between 64x64 and 128x32 pixels (for L1 and Mi9 experiments). Before starting the acquisition, we verified that the receptive fields of the cells were located on the stimulus arena by showing a search stimulus consisting of moving gratings.

Calcium imaging was performed as previously described in (Arenz et al., 2017). In brief: Images were automatically registered using horizontal and vertical translations to correct for the movement of the brain. Fluorescence changes (ΔF/F values) were then calculated using a standard baseline algorithm (Jia et al., 2011). Regions of interest (ROIs) were drawn on the average raw image by hand in the medulla layer M1 for L1 and in layer M10 for Mi9. For LPi neurons, ROIs were routinely chosen in the lobula plate, encompassing small regions with single to few axon terminals. Averaging the fluorescence change over this ROI in space resulted in a ΔF/F time course. Glutamate imaging was performed with the same settings as the calcium imaging experiments.

Visual stimulation for L1 and Mi9 experiments

The spatiotemporal response properties of the L1 and Mi9 columnar input elements were determined on a custom-built projector-based arena, as previously described in (Arenz et al., 2017). Stimuli were projected with 2 commercial micro-projectors (TI DLP Lightcrafter 3000) onto the back of an opaque cylindrical screen covering 180 ° in azimuth and 105 ° in elevation of the fly's visual field. The projectors refresh rate is 180 Hz (at 8 bit color depth). For all stimuli used here, we set the medium brightness to a 8-bit grayscale value of 50, which corresponds to a medium luminance of 55 ± 11 cd/m^2. Stimuli were rendered using a custom written software in Python 2.7.

Visual stimulation for LPi4-3 experiments with telescope

This technique has been previously described in (Haag et al., 2016). In brief: Antidromic illumination of the fly's head visualizes the hexagonal structure of the optical axes of the ommatidia (Franceschini, 1975; Schuling et al., 1989). Visual stimuli are generated on the AMOLED display (800x600 pixels, pixel size 15x15 mm, maximal luminance > 1500 cd/m^2; lambda = 530 nm; refresh rate 85 Hz) (SVGA050SG, Olightek). This allows to precisely position the stimuli onto single lamina cartriges. In order to prevent stimulus light from entering the photomultiplier of the two-photon micro-scope, light generated by the AMOLED display was filtered with a long-pass filter (514 LP, T: 529.4– 900 nm, AHF). The AMOLED display was controlled with MATLAB and the psychophysics toolbox (V3.0.11;(Brainard, 1997)).

White noise reverse-correlation

The analysis of spatial receptive fields was previously described in (Arenz et al., 2017). For the input elements, spatiotemporal receptive fields were calculated following standard reverse-correlation methods (Dayan and Abbott, 2013; French, 1976). First, the mean value was subtracted from the raw signals of single ROIs by using a low-pass filtered version of the signal (Gaussian filter with 120 seconds standard deviation) as a baseline for a ΔF/F-like representation of the signal.
The stimulus-response reverse correlation function was calculated as:

$$K(x,\tau) = \int_0^T dt\, S(x, t-\tau) \cdot R(t)$$

with S for the stimulus and R for the response of the neuron. The resulting spatiotemporal fields were normalized in z-score. Only receptive fields with peak amplitudes above 10 standard deviations from the mean were taken for further analysis (for Mi9-GCaMP6f the threshold

was lowered to 7). Cross-sections through the receptive fields along the space axis were fit with a Gaussian function to determine the position of the peak (Suppl. Fig. 1 E-F).

Gaussian noise stimulus

The same stimulus was used in (Arenz et al., 2017). In brief: The stimulus consisted of 64 vertical bars covering an angle of 180° in total. The intensity of each bar fluctuated randomly around a mean intensity of 50 on the 8-bit grayscale of the display. The intensities were drawn from a Gaussian distribution with a standard deviation of 25% contrast. In time, the stimulus was low-pass filtered with a Gaussian window with approximately 22ms standard deviation, which restricted the frequency content of the stimulus to frequencies below 10Hz. For Mi9-GCaMP6f imaging, similarly, the time window was 45ms long, covering frequencies until up to 5Hz.

Spatial receptive field

The analysis of spatial receptive fields was previously described in (Arenz et al., 2017). In brief: One-dimensional spatial receptive fields are cross-sections through the peak of the spatiotemporal receptive fields along the space axis and are averaged over the 12 samples (200ms) around the peak. For both L1 and Mi9 we found a small-field, antagonistic center-surround organization of the spatial receptive field using the vertical white noise stimulus.
The black dashed lines in Suppl. Fig 1 represents a Mexican hat function (Difference of Gaussian). Mathematically such a function can be described as follows:

$$RF_{1D}(\varphi) = e^{-\frac{1}{2}\frac{\varphi^2}{\sigma_{cen}{}^2}} - A_{rel} \cdot e^{-\frac{1}{2}\frac{\varphi^2}{\sigma_{sur}{}^2}}$$

with φ as azimuth, σ_{cen} and σ_{sur} as the standard deviations of center and surround, respectively, and $A_{rel} = A_{sur}/A_{cen}$ the relative strength of the surround in relation to the amplitude of the center Gaussian (which is normalized to 1).

Temporal receptive field

The analysis of temporal receptive fields was previously described in (Arenz et al., 2017). In brief: The time-reversed impulse responses shown in Figure 3 are cross-sections through the center of the spatiotemporal receptive fields along the time axis and are averaged over the three center pixels. For the determination of the time constants (tau), we sought to describe the response characteristic of each cell with a simplified model that catches the main properties. For that, we fitted simple 1st$_{st}$ order filters (e.g. 1st order low-pass for Mi9; 1st order bandpass for L1) to the impulse responses of all cells.
The model fit in Suppl. Fig 2 (grey lines) was performed by low-pass filtering the measured iGluSnFR response of each neuron type (L1, Mi9, LPi) with a 1st order low-pass filter and optimizing the time-constant such that the difference between the low-pass filtered signal and the measured calcium response of the neurons was minimal. The fitting procedure was implemented using standard least square algorithms (SciPy 0.19).

Immunohistochemistry

Fly brains were dissected in ice-cold 0.3% PBST and fixed in 4% PFA in 0.3% PBST for 25 min at room temperature. Subsequently, brains were washed 4-5 times in 0.3% PBST and blocked in 10% normal goat serum (NGS) in 0.3% PBST for 1 hour at room temperature. Primary antibodies used were mouse anti-bruchpilot brp (nc82, Developmental Studies

Hybridoma Bank, 1:20) and rabbit anti-VGlut (courtesy of H. Aberle, 1:500). Secondary antibodies used were: goat anti-mouse ATTO 647N (Rockland, 1:300) and goat anti-rabbit Alexa Fluor 568 (Life Technologies, 1:300). Myr::GFP-labeled cells were imaged natively without antibody staining. 5% NGS was added to all antibody solutions and both primary and secondary antibodies were incubated for at least 48 hours at 4°C.
Brains were mounted in Vectashield Antifade Mounting Medium (Vector Laboratories) and imaged on a Leica TCS SP8 confocal microscope.

Supplemental References

Brainard, D.H. (1997). The psychophysics toolbox. Spat. Vis. 10, 433–436.

Franceschini, N. (1975). Sampling of the visual environment by the compound eye of the fly: Fundamentals and applications. Photoreceptor Opt. 98–125.

Jia, H., Rochefort, N.L., Chen, X., Konnerth, A. (2011). In vivo two-photon imaging of sensory-evoked dendritic calcium signals in cortical neurons. Nat. Protoc. 6, 28–35.

Pologruto, T.A., Sabatini, B.L., Svoboda, K. (2003). ScanImage: Flexible software for operating laser scanning microscopes. Biomed. Eng. Online 2.

Schuling, F.H., Mastebroek, H.A.K., Bult, R., Lenting, B.P.M. (1989). Properties of elementary movement detectors in the fly *Calliphora erythrocephala*. J. Comp. Physiol. A 165, 179–192.